Lasers in Medical Science (2020) 35:43–49
https://doi.org/10.1007/s10103-019-02768-7

ORIGINAL ARTICLE

Probing deep tissues with laser-induced thermotherapy using near-infrared light

Alexandre Lopes[1,2] · Ricardo Gomes[3,4] · Marta Castiñeras[3] · João M. P. Coelho[3,4] · José Paulo Santos[1,2] · Pedro Vieira[1]

Received: 11 October 2018 / Accepted: 6 March 2019 / Published online: 17 May 2019

Abstract

Optically tunable gold nanoparticles have been widely used in research with near-infrared light as a means to enhance laser-induced thermal therapy since it capitalizes on nanoparticles' plasmonic heating properties. There have been several studies published on numerical models replicating this therapy in such conditions. However, there are several limitations on some of the models which can render the model unfaithful to therapy simulations. In this paper, two techniques of simulating laser-induced thermal therapy with a high-absorbing localized region of interest inside a phantom are compared. To validate these models, we conducted an experiment of an agar-agar phantom with an inclusion reproducing it with both models. The phantom was optically characterized by absorption and total attenuation. The first model is based on the macroperspective solution of the radiative transfer equation given by the diffusion equation, which is then coupled with the Pennes bioheat equation to obtain the temperature. The second is a Monte Carlo model that considers a *stochastic* solution of the same equation and is also considered as input to the Pennes bioheat transfer equation which is then computed. The Monte Carlo is in good agreement with the experimental data having an average percentage difference of 4.5% and a correlation factor of 0.98, while the diffusion method comparison with experimental data is 61% and 0.95 respectively. The optical characterization of the phantom and its inclusion were also validated indirectly since the Monte Carlo, which used those parameters, was also validated. While knowing the temperature in all points inside a body during photothermal therapy is important, one has to be mindful of the model which fits the conditions and properties. There are several reasons to justify the discrepancy of the diffusion method: low-scattering conditions, absorption, and reduced scattering are comparable. The error bars that are normally associated when characterizing an optical phantom can justify also a part of that uncertainty. For low-size tumors in depth, one may have to increase the light dosage in photothermal therapies to have a more effective treatment.

Keywords Phototherapy · Photothermal therapy · Monte Carlo · Diffusion approximation · Near-infrared light

Introduction

Breast cancer remains the leading killer cancer in middle-aged women around the world [16]. Despite recent advances in therapy and diagnosis, cancer continues to be a difficult disease to treat. Depending on its location, stage, or whether it became resistant to the ongoing treatment, the therapies can also change. Therefore, it is imperative that the resources the oncologist has to tackle this disease be numerous and diverse. In this work, we study near-infrared photothermal therapy (PTT), which allows non-ionizing radiation to diffuse inside tissue and cause low-temperature elevation [12, 15]. When compared to the most conventional therapies like surgery and chemotherapy, it is non-invasive and produces minimal damage to healthy tissue. A fraction of photon energy is absorbed and converted into heat, depending on tissue properties, which can destroy malignant tissue through processes like coagulation or hyperthermia if the achieved temperature and time of exposure at that temperature is sufficient [3]. A limiting factor in this process is large optical scattering in biological tissue which imposes restrictions on how deep one can heat a predetermined region of interest. With the advent of gold nanoparticles (GNP) in medicine, there is a promising opportunity to bypass such limitations.

✉ Alexandre Lopes
an.lopes@campus.fct.unl.pt

Extended author information available on the last page of the article.

Gold nanoparticles have tunable high-absorption properties in the NIR regions that allow local higher absorbed energy. Several authors [5, 6, 20, 26] report a temperature change at up to 3 cm in depth when using these particles while no temperature change was observed without them. This increase in temperature caused by exogenous contrast agents changes the rate of deposited heat which in turn is influenced by irradiation conditions and tissue properties that ultimately influence the therapy's success [25].

A myriad of cell-damaging effects can be observed starting from $\sim$ 39 °C where protein denaturation happens. Depending on the time of exposure, these effects can do reversible or irreversible damage to cells [12, 15, 21]. Hence, a precise temperature control is crucial since it is impossible to have probes to measure the temperature in all spaces. Consequently, it is important to have models that can mimic the illumination conditions and tissue properties, and allow an accurate temperature representation.

Among the many light models already developed, two stand out for being the most used in the community: diffusion model and Monte Carlo. Monte Carlo simulations give a stochastic representation of the solution to the radiative transfer equation (RTE), which is the equation that governs how light propagates inside biological tissue [27]. The diffusion equation can be obtained from the RTE considering some of its parameters as first-order spherical harmonic expansions which allow only isotropic and first-order anisotropic terms. In practice, this imposes restrictions on the conditions in which this theory is valid, i.e., on tissues with low absorption and high scattering properties [25].

The studies that are published using nanoparticles can be separated into two categories. There are some approaches when using gold nanoparticles in the literature that consider an homogeneous mixture of a solution and gold nanoparticles and replicate the temperature or irradiance with simulations [24, 26]. Other approaches consider two layers of tissue stacked with and without the presence of gold nanoparticles [5, 6]. Depending on the number of gold nanoparticles used, the optical properties of the tissue vary significantly to a point where absorption is comparable to scattering [19], which might render the diffusion theory ineffective. In this work, we will address this problem using an agar phantom with an inclusion that mimics this condition. First, the conventional method of measuring some of the phantoms' optical properties is presented. After, an experiment is conducted in which the phantom is irradiated and the temperature is measured with a thermocouple inside the phantom.

The numerical methods consider the light distribution using diffusion theory and Monte Carlo, which is considered the gold standard to model light [27]. To model the heat transfer mechanism, we choose the Pennes bioheat equation [18] that reproduces well the temperature inside a phantom [25].

In this paper, we present a study with a nanoparticle-based inclusion in a phantom far from its surface. To the best of the author's knowledge, this study is not presented elsewhere and is important since the nanoparticles aggregate around a tumor of finite size and other experiments present in-depth homogeneous mediums with nanoparticles [6]. We also characterize the optical properties of the mediums considered and the irradiation experiment.

Mathematical formulation

The models of optical and thermal propagations of light and heat through the tissue are presented in this section. In the first part, we consider the diffusion theory and Monte Carlo simulations to solve the radiative transfer equation, while the Pennes bioheat transfer equation is considered to model the heat propagation mechanism.

The diffusion equation with a constant wave source at its border is defined as [2]:

$$-\nabla \cdot \kappa(\mathbf{r})\nabla\phi(\mathbf{r}) + \mu_a(\mathbf{r})\phi(\mathbf{r}) = 0, \mathbf{r} \in \Omega, \tag{1}$$

where $\kappa = 1/(3(\mu_s' + \mu_a))$ is the diffusion coefficient, μ_a the absorption coefficient, μ_s' is the reduced scattering coefficient, ϕ the fluence rate, Ω its domain, and position vector $\mathbf{r}$. The fluence rate boundary conditions between phantom and exterior are defined by:

$$\phi(\mathbf{m}) + 2\xi(c)\kappa(\mathbf{m})\frac{\partial\phi(\mathbf{m})}{\partial\nu} = q(\mathbf{m}), \mathbf{m} \in \partial\Omega, \tag{2}$$

where the term $\xi(c)$ represents the refractive boundary mismatch between different regions, $\partial\nu$ represents the outward boundary normal, q is the source distribution at the boundary $\partial\Omega$, and $\mathbf{m}$ the position vector restricted to $\partial\Omega$. This model is derived under two premises: it is valid in high diffusive versus absorbing tissues and it is not valid near source points, where the gradient of fluence rate is not linear [25].

In a Monte Carlo simulation, each photon is simulated individually with a predetermined starting position, direction, and interaction mechanisms. In the near-infrared region, light either scatters or gets absorbed inside a homogeneous tissue. The scattering phase function of the radiative transfer equation in soft biological tissues can be modeled by the Henyey–Greenstein phase function [25]. At the boundaries, refraction and reflection are considered with Fresnel and Snell equations [8].

The laser-induced heating source term is described by $Q(\mathbf{r}, t) \equiv \mu_a(\mathbf{r}) \times \phi(\mathbf{r}, t)$ [25]. Since this term is external

to the heat generated in the body, we add it to the Pennes bioheat transfer equation as follows:

$$\rho c \frac{\partial T(\mathbf{r},t)}{\partial t} = \nabla \cdot (k(\mathbf{r})\nabla T(\mathbf{r},t)) + Q_m(\mathbf{r}) + Q(\mathbf{r},t) + \omega_b \rho_b c_b (T(\mathbf{r},t) - T_a), \mathbf{r} \in \Omega, \quad (3)$$

where ρ is the tissue density, c is the specific heat, $T(\mathbf{r},t)$ the temperature, $k(\mathbf{r})$ the thermal conductivity, Q_m metabolic heat rate, ω_b rate of blood perfusion, ρ_b density of blood, c_b blood's specific heat, and T_a body's temperature.

The convection heat transfer mechanism is also considered and is determined by Newton's law:

$$Q_c = h(T_\infty - T(\mathbf{m},t)), \mathbf{m} \in \partial\Omega, \quad (4)$$

where h is the convective heat transfer coefficient and T_∞ is the room temperature. Radiation, thermal evaporation, and/or phase change of tissue during the heat transfer process are not considered in the simulations.

Materials and methods

An agar-agar phantom was produced in two steps. First, a mixture of 1.0% agarose powder (Agar-Agar, Vahiné, France) in distilled water. The water was heated along with the agarose powder and mixed (at a mixing temperature of ≈ 90 °C) three times to ensure a homogeneous optical density of the gel. It was then left to cool off inside a 60×60×60 mm^3 cube using a cylinder of 15.5 mm in diameter to create a 5-mm-deep hole on top of the phantom. Once it cooled down to ambient temperature, the hole created by the cylinder was filled with two equal parts of agar and gold nanoparticles prepared according to [23]. The two were mixed at 35 °C since the gold nanoparticles had a biocoating in them. This proportion was used to not only ensure the gold nanoparticles were in a fixed place, but also to have a good balance between scattering and absorption. A 4-mm layer of agar-agar solution was added to the phantom. The final phantom is depicted in Fig. 1.

Determination of materials' properties

The optical properties of the gel and inclusion were measured using an integrating sphere (International Light, INS 250), a laser diode source (Roithner, RLTMDL-808-5W-5) 808-nm wavelength, and a spectrometer (Avaspec 2048, Avantes). The measured coefficients were the absorption coefficient and the total attenuation coefficient. Other optical properties such as anisotropy and refractive index were taken from literature [6, 11].

Similarly to the methods described in [17], the absorption coefficient (μ_a) was measured placing the cuvette with a sample of agar or nanoparticles and agar in the integrating sphere's center, and compared with a cuvette with distilled water. Coupled with the integrating sphere was the spectrometer whose signal was then deconvoluted from the laser wavelength distribution peaking at 808 nm. The absorption coefficient was determined using the equation $\mu_a = \frac{I_0 - I}{I_0}$, where I_0 is the measurement with distilled water, and I the signal measured with the sample solution.

To measure the attenuation coefficient (μ_t), a procedure similar to the one described in [17] was followed. Additionally, a 1-mm pinhole was placed in front of the detector and both were positioned 40 cm away from the sample. This procedure is reported to limit multiple scattering events to some extent [13, 14]. The Beer–Lambert equation was used to determine the attenuation coefficient, $\mu_t = -\log \frac{I}{I_0}$, where I is the measured signal of the cuvette with the sample and I_0 is the measured signal of the cuvette with distilled water. Each measurement was repeated 5 times to ensure consistency. The scattering coefficient was determined indirectly by the equation $\mu_s = \mu_t - \mu_a$. Table 1 shows the results of the two mixtures used in the phantom.

Experimental setup

The phantom was irradiated on the top surface of the box with a continuous-wave diode laser of 1.1-W power and a full width at half maximum (FWHM) of 7 mm, as

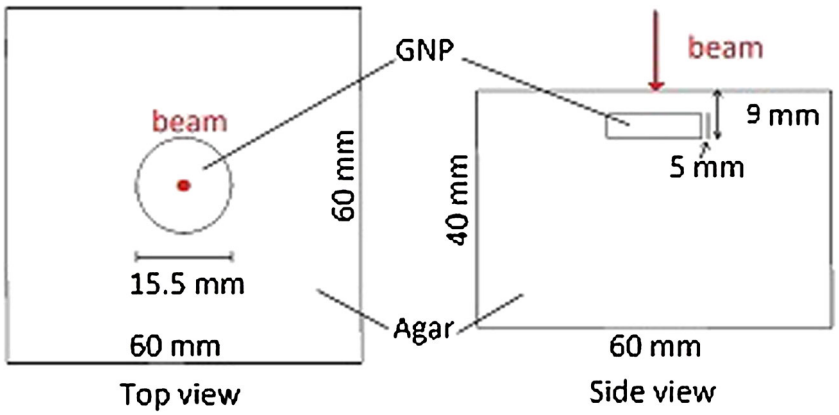

Fig. 1 Gel phantom setup. The laser beam entry position and direction are depicted in red. The main component (agar) is made of 1% agar and water, while the smaller component (GNP) is made of 1% agar, 10% GNP solution, and 89% water

Table 1 Measured optical properties of the agar gel phantom and a mixture of gold nanoparticles (GNP) and agar gel

Sample	μ_a (mm^{-1})	μ_t (mm^{-1})	μ_s (mm^{-1})
Gel	0.002	0.178	0.176
GNP	0.031	0.320	0.289

represented in Fig. 1. A multi-mode fiber and a collimator were used with the laser to provide a more portable and stable beam. Assuming a Gaussian laser beam profile [1], one can associate the FWHM to a beam diameter of 11 mm at the $1/e^2$ points of the distribution. Using the laser power and the beam diameter produces an irradiance at the Agar gel phantom's surface of 2.31 W/cm^2.

Temperatures were registered using a type K thermocouple (Labfacility, Z2-T-1M) and a thermocouple converter (Seneca K109TC) connected to a LabVIEW® interface and with a tunable data acquisition rate of 1 s. The thermocouple was placed on top of the cylinder, at 4 mm in depth. The constant wave laser was on for 706 s, then turned off. The radiation absorbed by thermocouple was taken into account and was subtracted from experimental results as suggested in [4]. The ambient temperature was measured at 22.9 °C and the temperature measured in the thermocouple the instant before the laser irradiation phase was 23.88 °C, which is considered the reference temperature when determining temperature change.

Simulations

Several software applications were used to compute the solution temperature distribution of the phantom. Along with the commercial software COMSOL Multiphysics® and MATLAB®, which were used to perform the data analysis. Iso2mesh [9] and GMSH [10] were used to build and characterize the meshed phantom. This mesh was used as an input in both TOAST++ [22] and the Monte Carlo software Mesh-based Monte Carlo [7]. Both of these codes are considered to be the state of the art in their own domain to determine the irradiance within biological tissue. One only needs to provide the laser parameters and the tissue's optical properties since the appropriate functions are already built in. All codes were run in a 8× Intel Core i7 4790 (4.0 GHz) CPU with 4× 4GB DDR3 1600 MHz.

The diffusion approximation software provides the selection of a Gaussian profiled source with $\sigma = 3.07$ mm, modelled as a Neumann source which considers it as a diffuse boundary current. The same laser profile and the standard deviation were selected in the Monte Carlo simulator. Ten million events were simulated. The output fluence rate of both programs was then used as the 3D heat source in COMSOL.

The temperature for both cases was computed by COMSOL Multiphysics®. The top surface transferred convective heat using the Newton convection heat transfer equation with the respective coefficient at 5 W K^{-1} m^{-2} [25], while the other surfaces were considered to be in thermal isolation. Although this latter consideration could be considered erroneous, its effect is significant only after the laser-on phase when the phantom is cooling down. The blood density and the metabolic heat coefficient of the Pennes bioheat equation were set to 0. This consideration converts the Pennes bioheat equation into the classical heat transfer equation. The density, heat capacity, and thermal conductivity coefficients of water were considered in this test.

The used optical parameters for the phantom are the following: absorption coefficient: μ_a 0.002 mm^{-1}, reduced scattering coefficient $\mu_s' = \mu_s(1-g) = 0.0176$ mm^{-1} an anisotropy (g) of 0.9 is assumed [6], refractive index = 1.33 [11]. The inclusion's optical properties differ from the previous ones on the absorption coefficient, which is $\mu_a = 0.031$ mm^{-1} and reduced scattering coefficient $\mu_s' = 0.029$ mm^{-1}, while the others are the same. This increase in optical absorption is considered a heat source within the phantom, modelled in COMSOL. Inside the inclusion, the absorption coefficient and the reduced scattering coefficient are comparable and can make the diffusion approximation ineffective.

Results and discussion

To check that both models work within reasonable agreement, a simulation was conducted. Consider a case in which both Monte Carlo and the diffusion approximation are effective; a homogeneous 2-cm-wide cube with the following optical properties: $\mu_a = 0.002$ mm^{-1}, $\mu_s' = 1.22$ mm^{-1}, $g = 0.9$, and refractive index of 1.33. A continuous-wave Gaussian near-infrared laser beam of power = 1.5 W and FWHM = 5 mm is aimed at one of the cube's side at the center for 180 s. Figure 2 shows a comparison between temperature increases of both simulators 1-mm deep of the irradiated side. One can observe the diffusion approximation is almost 1 K higher at 180 s between simulated temperatures which is caused by the different approaches of dealing with scattering anisotropy by the two models.

Figure 3 presents the comparison between experiment and simulation results given from Monte Carlo and diffusion theory. There are some variations in the measured temperature along time. The thermocouple probe has a higher absorption in the near infrared than the medium that surrounds it, which leads to accumulated energy that is diffused non-linearly. This fact can be confirmed since

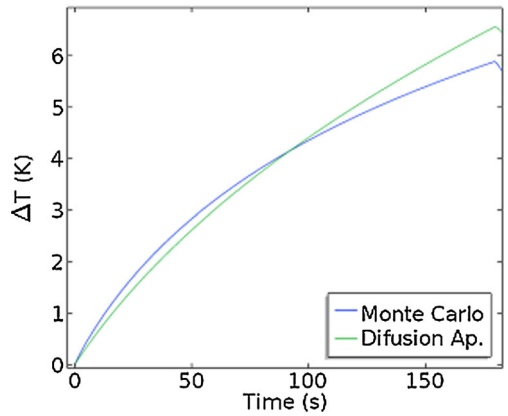

Fig. 2 Temperature increase comparison between Monte Carlo (blue) and the diffusion theory (green) simulators as a function of time, at a point located 1mm below the irradiated spot

the instant the irradiation phase stopped, this behavior was not observed. These variations decrease in amplitude using a smaller thermocouple probe since it would decrease its thermal capacity, as one can compare with the results from [4]. The average percentage difference between the Monte Carlo model is 4.5% and for the diffusion approximation 61%, while the correlation coefficient was of 0.98 and 0.95, respectively.

Both models are in good agreement with the experiment measurements. These results can be compared to, e.g., Elliot et al. [6] where this problem is explored in a similar experiment. Joined in a single phantom cylinder are two smaller cylinders with the same radius and with different optical properties and height. The diffusion approximation was used to model the experiment. The physical parameters for the finite element calculations were adjusted within the experimental error (± 10%) to optimize results. The average percentage difference and correlation coefficient were 4.5%

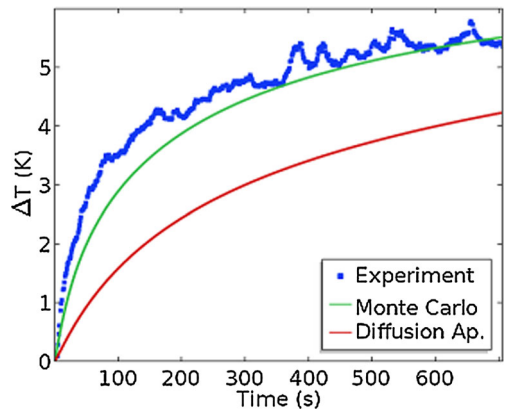

Fig. 3 Comparison of simulation and experimentally measured increase in temperature, 4 mm below surface. It shows temperature change as a function of time. Both models are shown in green and red and are compared with the experimental results shown in blue

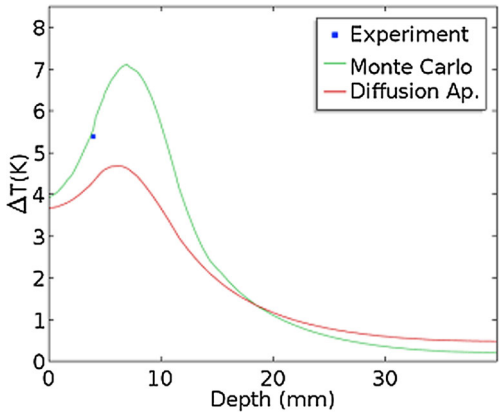

Fig. 4 Temperature increase at $t = 706$ s right before the laser was turned off. The x-axis represents an axis that is aligned with the laser beam axis, which is located at the center of two faces of the cube. The Monte Carlo simulation and diffusion approximation results are presented in green and red, respectively. The experimental point is shown in blue

and 0.99, respectively, for the similar conditions as for this experiment.

To quantify the impact of experimental uncertainty in the diffusion approximation, we changed the physical parameters, namely the reduced scattering and the absorption coefficients in the diffusion approximation model, by 20%. This change resulted in a decrease in the average percentage difference from 61 to 23%. Although this variation is far from the 4.5% reported in [6], this result highlights the model sensitivity on these parameters.

Figure 4 shows the temperature increase in depth along the axis that is aligned with the laser beam axis the second before the laser was shut down. The distribution of both models is slightly different. Using more thermocouple probes would allow a more comprehensive study of this distribution. When comparing it with similar temperature change distributions in other studies, such as [5, 6], increases in temperature greater than 10 K can be observed. This result suggests that the size of the inclusion with nanoparticles is a relevant component to temperature increase, along with irradiance as well as the inclusions' optical properties, density, and location inside tissue.

Conclusions

It is of crucial importance to know the temperature in every point inside the tissue when performing photothermal therapy to better control the light dosage delivered. We present two ways of simulating laser-induced thermal therapy in a specific experimental setup with a high-absorbing region of interest located at 4 mm in depth, and compared to experimental data. The two models are in reasonable agreement with the experiment results. The

Monte Carlo model has an average percentage difference of 4.5% when comparing it to experimental data, while the diffusion approximation is of 61%. Both models have correlation coefficients above 0.95. Also, results demonstrate that several inclusion parameters (size, optical properties, density, and location) affect the maximum temperature one can achieve.

Funding Information This work was partially supported by national funding by the Portuguese FCT - Fundação para a Ciência e Tecnologia through the projects PD/BD/105920/2014, UID/FIS/04559/2013(LIBPhys) and UID/BIO/00645/2019.

Compliance with Ethical Standards

Conflict of interest The authors declare that they have no conflict of interest.

References

1. Alda J (2003) Laser and Gaussian beam propagation and transformation. Encycloped Opt Eng 2013:999–1013. https://doi.org/10.1081/E-EOE 120009751
2. Arridge SR (1999) Optical tomography in medical imaging. Inverse Problems 15(2):R41. https://doi.org/10.1088/0266-5611/15/2/022
3. Brunetaud JM, Mordon S, Maunoury V, Beacco C (1995) Non-PDT uses of lasers in oncology. Lasers Med Sci 10(1):3–8. https://doi.org/10.1007/BF02133156
4. Cain CP, Welch AJ (1974) Thin-film temperature sensors for biological measurements. IEEE Trans Biomed Eng BME-21(5):421–423. https://doi.org/10.1109/TBME.1974.324415
5. Cheong SSK, Krishnan S, Cho SH (2008) Modeling of plasmonic heating from individual gold nanoshells for near-infrared laser-induced thermal therapy. Med Phys 36(6):4664–4671. https://doi.org/10.1118/1.2961677
6. Elliott AM, Stafford RJ, Schwartz J, Wang J, Shetty AM, Bourgoyne C, O'Neal P, Hazle JD (2007) Laser-induced thermal response and characterization of nanoparticles for cancer treatment using magnetic resonance thermal imaging. Med Phys 34(7):3102–3108. https://doi.org/10.1118/1.2733801
7. Fang Q (2010) Mesh-based Monte Carlo method using fast ray-tracing in Plucker coordinates. Biomed Opt Express 1(1):165–175. https://doi.org/10.1364/BOE.1.000165
8. Fang Q, Boas D (2009) Monte Carlo simulation of photon migration in 3D turbid media accelerated by graphics processing units. Opt Express 17(22):20178–20190. https://doi.org/10.1364/OE.17.020178
9. Fang Q, Boas DA (2009) Tetrahedral mesh generation from volumetric binary and grayscale images. In: Proceedings - 2009 IEEE international symposium on biomedical imaging: from nano to macro. ISBI 2009, pp 1142–1145. https://doi.org/10.1109/ISBI.2009.5193259
10. Geuzaine C, Remacle JF (2009) Gmsh: a three-dimensional finite element mesh generator with built-in pre-and post-processing facilities. Int J Numer Methods Eng 79(11):0, 1309–1331. https://doi.org/10.1002/nme.2579
11. Jacques SL (2013) Optical properties of biological tissues: a review. Phys Med Biol 58(11):R37. https://doi.org/10.1088/0031-9155/58/11/R37
12. Jaque D, Martínez Maestro L, del Rosal B, Haro-Gonzalez P, Benayas A, Plaza JL, Martín Rodriguez E, García Solė J (2014) Nanoparticles for photothermal therapies. Nanoscale 6(16):9494–9530. https://doi.org/10.1039/c4nr00708e
13. Kim A, Wilson BC (2010) Measurement of ex vivo and in vivo tissue optical properties: methods and theories. In: Optical-thermal response of laser-irradiated tissue. Springer, Netherlands, pp 267–319, https://doi.org/10.1007/978-90-481-8831-48
14. Marchesini R, Bertoni A, Andreola S, Melloni E, Sichirollo aE (1989) Extinction and absorption coefficients and scattering phase functions of human tissues in vitro. Appl Opt 28(12):2318–24. https://doi.org/10.1364/AO.28.002318. http://www.ncbi.nlm.nih.gov/pubmed/20555518
15. Niemz MH (1996) Laser-tissue interactions. Springer, Berlin. http://link.springer.com/10.1007/978-3-662-03193-3. https://doi.org/10.1007/978-3-662-03193-3
16. Organization WH (2013) Women's health. http://www.who.int/mediacentre/factsheets/fs334/en/
17. Patterson MS, Wilson BC, Wyman DR (1991) The propagation of optical radiation in tissue. II: optical properties of tissues and resulting fluence distributions. Lasers Med Sci 6(4):379–390. https://doi.org/10.1007/BF02042460
18. Pennes HH (1998) Analysis of tissue and arterial blood temperatures in the resting human forearm. 1948. J Appl Physiol (Bethesda Md. : 1985) 85:5–34. DOI 9714612
19. Phadnis A, Kumar S, Srivastava A (2016) Numerical investigation of thermal response of laser-irradiated biological tissue phantoms embedded with gold nanoshells. J Therm Biol 61:16–28. https://doi.org/10.1016/j.jtherbio.2016.08.002
20. Reynoso FJ, Lee Cd, Cheong Sk, Cho SH (2013) Implementation of a multisource model for gold nanoparticle-mediated plasmonic heating with near-infrared laser by the finite element method. Med Phys 40(7):073301. https://doi.org/10.1118/1.4808361
21. Sapareto SA, Dewey WC (1984) Thermal dose determination in cancer therapy. Int J Radiation Oncol Biol Phys 10(6):787–800. https://doi.org/10.1016/0360-3016(84)90379-1
22. Schweiger M, Arridge S (2014) The Toast++ software suite for forward and inverse modeling in optical tomography. J Biomed Opt 19(4):040801. https://doi.org/10.1117/1.JBO.19.4.040801
23. Silva CO, Rijo P, Molpeceres J, Ascensão L, Roberto A, Fernandes AS, Gomes R, Pinto Coelho JM, Gabriel A, Vieira P, Reis CP (2016) Bioproduction of gold nanoparticles for photothermal therapy. Therapeutic Deliv 7(5):287–304. https://doi.org/10.4155/tde-2015-0011
24. Vera J, Bayazitoglu Y (2009) A note on laser penetration in nanoshell deposited tissue. Int J Heat Mass Transf 52(13-14):3402–3406. https://doi.org/10.1016/j.ijheatmasstransfer.2009.02.014
25. Welch AJ, Van Gemert MJC (2011) Optical-thermal response of laser-irradiated tissue, vol 2. Springer, Dordrecht. https://doi.org/10.1007/978-90-481-8831-4
26. West JL, Hirsch LR, Stafford RJ, Bankson JA, Sershen SR, Rivera B, Price RE, Hazle JD, Halas NJ, West JL (2003) Nanoshell-mediated near-infrared thermal therapy of tumors under magnetic resonance guidance. Proc Natl Acad Sci 100(23):13549–13554. https://doi.org/10.1073/pnas.2232479100
27. Yao R, Intes X, Fang Q (2016) Generalized mesh-based Monte Carlo for wide-field illumination and detection via mesh retessellation. Biomed Opt Express 7(1):171. https://doi.org/10.1364/BOE.7.000171

Affiliations

Alexandre Lopes[1,2] · Ricardo Gomes[3,4] · Marta Castiñeras[3] · João M. P. Coelho[3,4] · José Paulo Santos[1,2] · Pedro Vieira[1]

1 Department of Physics, Faculdade de Ciências e Tecnologia da Universidade Nova de Lisboa, Monte da Caparica, Portugal

2 LIBPhys, Faculdade de Ciências e Tecnologia da Universidade Nova de Lisboa, Monte da Caparica, Portugal

3 Laboratório de Óptica, Lasers e Sistemas, Faculdade de Ciências, Universidade de Lisboa, Lisboa, Portugal

4 Instituto de Biofísica e Engenharia Biomédica, Faculdade de Ciências, Universidade de Lisboa, Lisboa, Portugal